ORIGINAL RESEARCH ARTICLE

Elaboration and Characterization of Ni (NPs)-PANI Hybrid Material by Electrodeposition for Non-Enzymatic Glucose Sensing

D. Lakhdari[1,2] · A. Guittoum[3] · N. Benbrahim[2] · O. Belgherbi[1] · M. Berkani[4] · L. Seid[5] · S. A. Khtar[6] · M. A. Saeed[6] · N. Lakhdari[4]

Abstract

A two-step process was used to prepare a nickel-polyaniline nanocomposite (Ni (NPs)-PANI). The first step consisted of the electrodeposition of polyaniline (PANI) in the form of thin films on fluorine-doped tin oxide (FTO) substrates from a solution of aniline, lithium perchlorate, and sulfuric acid at a pH of 0.5. In the next step, the obtained Ni (NPs) were deposed in this polyaniline films. The structural, morphological, and electrocatalytic properties of the prepared nanocomposites were then investigated. X-ray diffraction (XRD) confirmed the cubic structure of the nanocomposites, and Fourier-transform infrared spectroscopy (FTIR) indicated the existence of nickel and polyaniline in the prepared nanocomposites. Morphological analysis carried out through SEM revealed that the nanocomposites exhibit uniform dispersion of nickel nanoparticles into the polyaniline matrix. Amperometry and cyclic voltammetry were employed to investigate the electrocatalytic glucose oxidation behavior of the nanocomposite electrode in the alkaline medium. The prepared nickel-polyaniline nanocomposite electrode exhibited high sensitivity (278.8 μA mM^{-1} cm^{-2}) in a range from 0.02 to 1 mM at a sufficiently fast response time of 3 s and a low glucose detection limit of 1 μM (S/N = 3). A cost-effective and straightforward synthesis procedure to prepare Ni (NPs)-PANI nanocomposite would make this material an efficient glucose sensor with appropriate stability, higher reproducibility, and excellent sensitivity.

✉ D. Lakhdari
d.lakhdari@crti.dz

1 Research Center in Industrial Technologies CRTI, P.O. Box 64, 16014 Cheraga, Algiers, Algeria

2 Laboratoire de Physique et Chimie des Matériaux (LPCM), Université Mouloud MAMMERI de Tizi Ouzou, RP 15000 Tizi Ouzou, Algeria

3 Nuclear Research Centre of Algiers, 2 Bd Frantz Fanon, Bp 399, Alger-Gare, Algiers, Algeria

4 Laboratoire Biotechnologies, Ecole Nationale Supérieure de Biotechnologie, Ville Universitaire Ali Mendjeli, BP E66 25100 Constantine, Algeria

5 Laboratoire d'Energétique et d'Electrochimie du Solide (LEES), Département de Génie Des Procédés, Faculté de Technologie, Universite Sétif-1, Sétif, Algeria

6 Department of Physics, University of Education, Lahore 54770, Pakistan

Introduction

Glucose detection is highly significant in many fields including clinical diagnostics,[1] pharmaceutical analysis,[2] the food industry,[3] and biotechnology.[4,5] Enzyme-based glucose oxidase (GOD) sensors have been studied extensively for the detection of glucose levels in the blood and in food products; among the remarkable properties of glucose sensors, they exhibit high sensitivity and provide good selectivity. The main factors considered as disadvantages limiting the application of GOD-based biosensors are poor reproducibility, thermal and chemical instability, and high cost.[6] These issues can be addressed by using non-enzymatic glucose sensors, which have been widely studied for detecting glucose levels in the blood and in food products. The main advantages of these glucose-based sensors are their proven high sensitivity and selectivity; however, GOD-based biosensors may be less reproducible, which unfortunately limits their application. In recent years, many studies have focused

on investigating direct electrocatalysis to minimize the disadvantages of enzymatic biosensors.[7]

Many non-enzymatic electrode materials have been investigated, using noble metal nanomaterials[8–14] and corresponding alloys,[15] composite materials,[16,17] and transition metals and their alloys.[18] Recently, the incorporation of metal nanoparticles on polyaniline, polythiophene, or polypyrrole as electrically conducting polymers has been widely studied.[19,20] This interesting range of materials are considered promising in a few fields of catalysis and electrocatalysis, due to the ability of metallic nanoparticles to disseminate in polymers such as polyaniline (PANI), which provides excellent efficiency and reproducibility as an electrode with high electrical conductivity and as a unique redox material used for various biosensors.[21,22]

Recently, Ni-based systems have attracted special attention for the construction of diagnostic sensors due to Ni's natural abundance, its remarkable ability to catalyze glucose oxidation,[23–27] large surface area, and high concentration of electrocatalytic active sites.[28–33]

Therefore, this study aims to use a thin polyaniline film on transparent conductive glass (FTO) substrate as a support, which uses inexpensive metal nanoparticles. This system exhibits catalytic behavior against non-enzymatic glucose oxidation.

Experimental Details

Preparation of Nickel-Polyaniline Nanocomposite (Ni (NPs)-PANI) Electrode

Electrodeposition of the Ni (NPs)-PANI nanocomposite was performed via thin films on FTO substrates, having a size of 1×1 cm. Two electrodes were used, in which a saturated calomel electrode and a platinum wire were used as reference (RE) electrodes, respectively.

The analytical reagents used in the experiments were purchased from Sigma-Aldrich, and the work solutions were prepared using deionized water. A radiometer potentiostat-galvanostat PGZ 301 controlled by Volta Master software was used for electrochemical measurements.

Analysis

The structural and morphological properties of the nanocomposites were analyzed using a Bruker D8 Discover X-ray diffractometer with CuKα radiation ($\lambda = 1.79$ Å) and a scanning electron microscope (SEM) (ZEISS GeminiSEM 300), respectively. The surface topography of the nanocomposites was studied using atomic force microscopy

(AFM), and statistical analysis was performed by PicoScan 5.3 software from Molecular Imaging in order to determine the root-mean-square roughness. A Shimadzu IRAffinity-1S spectrometer was used to carry out Fourier-transform infrared (FTIR) spectroscopy (400 to 4000 cm^{-1}). A UV-visible (UV-vis) spectrophotometer (Shimadzu UV-1800) and KLA Tencor D-500 profilometer were employed for optical analysis and to measure the thickness of the PANI thin film, respectively.

Electro-Polymerization and Deposition of Ni (NPs)-PANI Electrode

The FTO substrates were used as working electrodes, which were thoroughly cleaned via sonication in acetone, ethanol, and water sequentially for 15 min. The clean working electrode was then transferred immediately to the electrochemical cell containing a solution of aniline (0.1 M), sulfuric acid (0.5 M), and lithium perchlorate (0.1 M). The nanoparticles of nickel were electrodeposited on the PANI layer with nickel sulfate (0.25 M), sodium sulfate (1 M), 0.4 M boric acid, H_3BO_3, and 0.012 M saccharin.

Electrodeposition of Polyaniline Films on FTO

The PANI film was prepared by the electrodeposition method. In this technique, fluorine-doped tin oxide (FTO) substrates were used to deposit PANI film with cyclic voltammetry between −0.2 and 1 V at 10 mV s^{-1} in an electrolytic solution (0.1 M aniline, 0.5 M H_2SO_4 and 0.1 M $LiClO_4$). Figure 2 depicts the CV (cyclic voltammogram) of the FTO glass electrode in an acidic solution containing aniline monomer (0.1 M). The voltammograms were recorded after one and five cycles under the following conditions: the potential was scanned from −0.2 to +1 V/SCE at 10 mV s^{-1}.

The experimental voltammetry curve observed during the first cycle (Fig. 1a) showed that the existence of monomer oxidation improves the current density at 0.85 V in the positive scan. In the negative scan, a current loop appeared due to nucleation of the polymer, towards the formation of the thin film. At 0.4 V, a cathodic peak is evident corresponding to the reduction of the polymer. From Fig. 1b it should be noted that six anodic peaks were detected, i.e. three peaks at 0.167/0.418/0.780 V/ECS and three peaks at −0.056/0.388/0.616 V/ECS, by sweeping the negative potential, which correspond to the different states of the polymer. The cyclic voltammogram results revealed a remarkable shift for the peak oxidation and reduction potentials, which allowed a significant improvement in the current intensity, especially for a two-redox system. This observation confirms

Fig. 1 Cyclic voltammograms of polyaniline growth on FTO substrate in presence of 0.5 M H_2SO_4 + 0.1 M $LiClO_4$ with different cycle numbers: (a) 1 cycle, (b) 5 cycles at 10 mV/s.
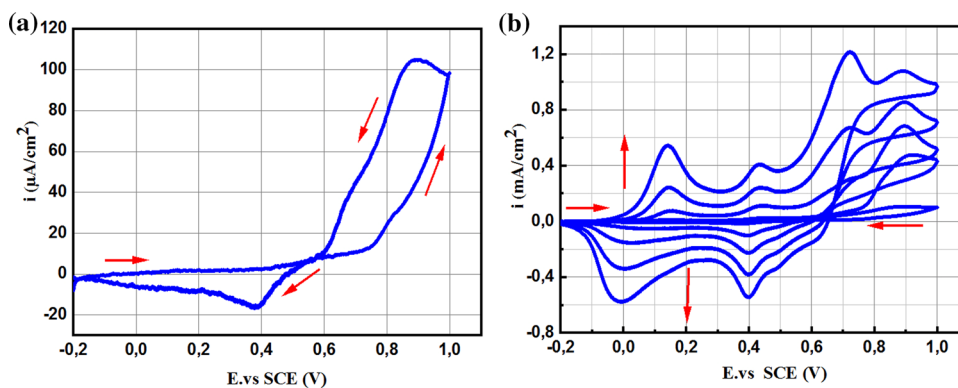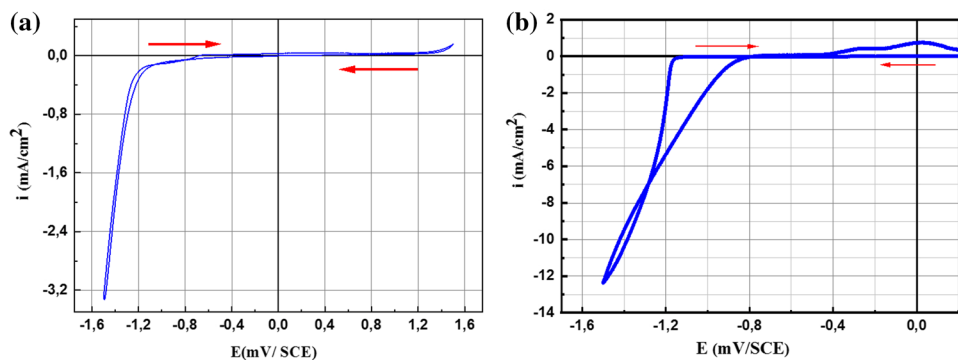

Fig. 2 Cyclic voltammograms of FTO electrodes in aqueous solutions containing 0.4 M H_3BO_3, 0.012 M saccharin, 1 M Na_2SO_4, without (a) and with 0.25 M $NiSO_4$.6 H_2O (b).

that the PANI layer, characterized by its electrochemically active and conductive properties, can develop on the surface of the electrode.[34] The electropolymerization process resulted in a green thin film with uniform distribution.

Incorporation of Ni nanoparticles in PANI thin film

Cyclic voltammetry was used to study the deposition potential for Ni. Figure 2 reveals the CV of the FTO electrode recorded in solutions containing 0.012 M saccharin, 0.4 M H_3BO_3, and 1 M Na_2SO_4 (blank solution, without electroactive species), and in 0.25 M $NiSO_4$.6H_2O. The scan rate was 20 mVs^{-1}. For the blank solution (Fig. 2a), the FTO electrode appears to have significant stability between −1.4 and 1.4 V. At the negative side, a reduction peak appeared at around −1 V. This peak corresponds to a diffusion-limited reduction of protons. Figure 2b shows the voltammetry curve of nickel at a concentration of 0.25 M where the oxidation peak is hardly detected at −0.13 V and is related to the dissolution of nickel, whereas the reduction peak has appeared at −0.84 V.

Chronoamperometry was investigated to deposit Ni nanoparticles on the PANI surface using a constant potential. Figure 3 shows current transients of Ni nanoparticles electrodeposited on PANI thin film at −1.36 V for 1 min
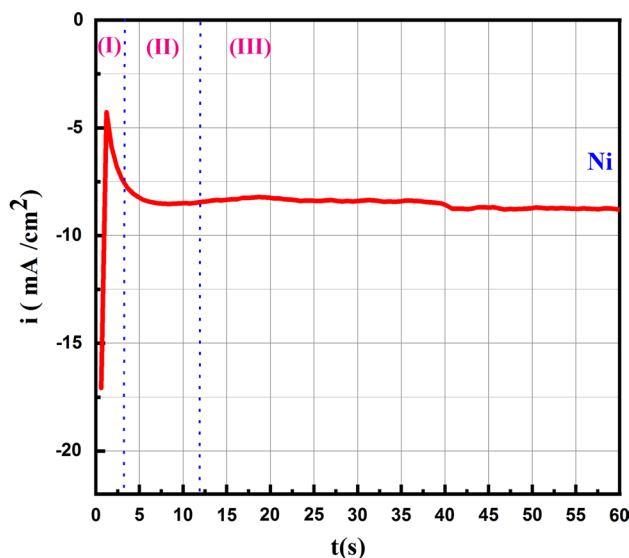

Fig. 3 Electrodeposition diagrams of Ni nanoparticles on PANI thin film at −1.36V, t = 60 s.

initially; the results exhibit an increase in the values of the current transients to the maximum because of the charge of double layers and generated germs on active sites. Thus, current saturation was observed due to the increasing number of nuclei in the electrochemical diffusion system.

Results and Discussion

Characterization of Ni (NPs)-PANI Electrode by X-ray Diffractometry

X-ray diffraction (XRD) analysis of PANI and the preparation of Ni (NPs)-PANI thin films on FTO glass by electrodeposition are shown in Fig. 3. XRD peaks of the FTO-coated glass substrate are marked as "*". The diffraction peak emerges at 2θ values of 16.27°, 21.77°, and 26.7° for PANI and Ni (NPs)-PANI electrodes, corresponding to semi-crystalline polyaniline thin films (Fig. 3a).[35] In addition, Fig. 3b shows the diffraction peak of Ni (NPs) which was observed at a 2θ value of 52.28°, which corresponds to the FCC Ni lattice structure, with the most intense diffraction peak corresponding to the (111) plane Fig. (4). The crystallite size can be calculated by the Debye-Scherrer equation using the XRD results (Eq. 1).
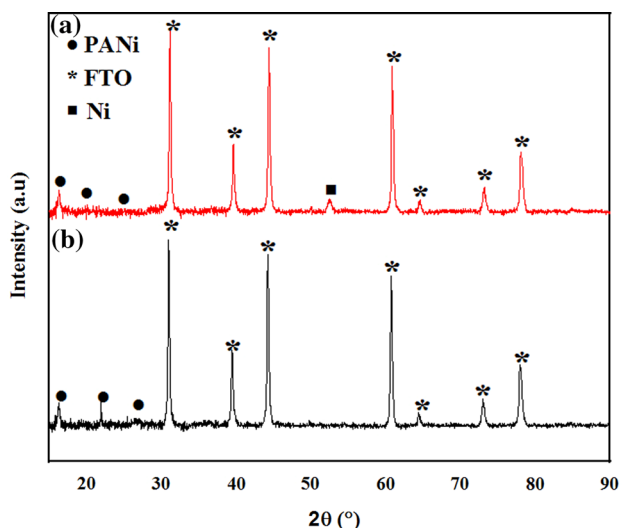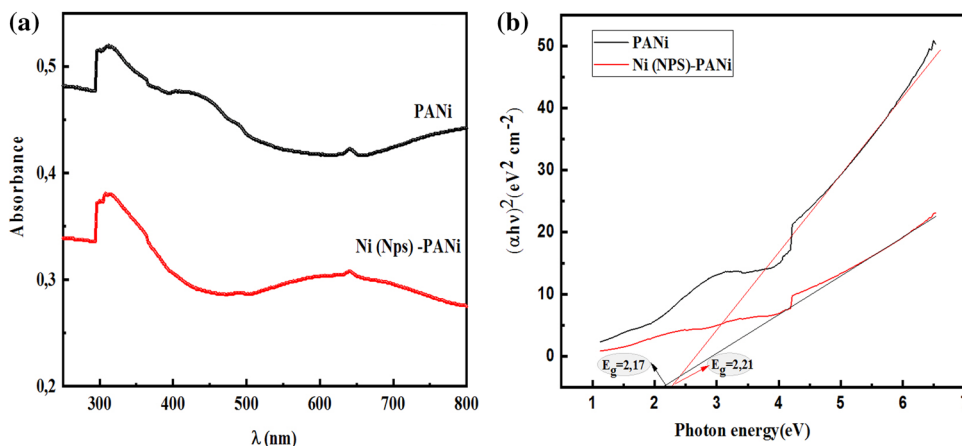
$$D = (0.9\,\lambda)/\beta\cos\theta \tag{1}$$

Fig. 4 Characterization of (a) PANI thin film, (b) Ni (NPS)-PANI by X-ray diffractometry

The grain size for Ni (NPs) is in the range of 17.85 nm. Wang et al. previously reported the same growth of Ni by electrodeposition along its preferred orientation.[36]

Optical Properties of Composites

UV–Vis spectroscopy was used to study the interaction between the PANI and Ni nanoparticles deposited on the FTO substrate (Fig. 5a). As can be seen in Fig. 5a, three particular peaks of polyaniline at 311, 411, 776 nm are attributed to π π*, polaron-π* and π- polaron transitions, respectively.[37] This illustrates that the above-mentioned PANI films were in emeraldine salt form.[38] Therefore, in comparison to the peaks of the PANI film, we observed a remarkable change in all three absorption peaks, which are shown in Fig. 5a for Ni (NPs)-PANI, and are as follow: 343, 432, 651, implying the existence of interactions between metal ions and PANI chains.[38] The plot of $(\alpha h\upsilon)^2$ versus $(h\upsilon)$ (where α is the absorption coefficient of films, h is blank constant, and υ is frequency) for PANI and Ni (NPs)-PANI electrodes is shown in Fig. 5b. It should be noted that the band gap E_g decreased from 2.21 to 2.11 eV with the nickel i incorporation.

FTIR Spectra

The FTIR results of Ni (NPs)-PANI electrode formation are illustrated in Fig. 6 (IR spectra of PANI thin film and Ni (NPs)-PANI nanocomposite, respectively). The two absorption bands at 1560 and 1490 cm^{-1} refer to the stretching vibrations of N=Q=N and N-B-N rings, respectively. The C–N stretching vibration covers an absorption band at 1300 cm^{-1}, while characteristic peaks of the B–NH–Q, B–NH–B, and C–H bonds of benzene rings appeared at 1109 and 800 cm^{-1}, respectively. In B–NH–Q, B refers to benzene-type and Q refers to the quinine-type rings.[33, 34] The incorporation of Ni^{2+} in PANI is evident from the shifting of the band assigned to the N–H bending

Fig. 5 UV-vis spectra of (a) PANI and Ni (NPs)-PANI electrode, optical band gap (αhν)2 versus photon energy (hν) plots of PANI thin film and (b) Ni (NPS)-PANI.

mode at 1400 cm^{-1} to 1303 cm^{-1}, which indicates interaction with the nitrogens atoms of the PANI. [37]

Morphological Characterization

Chronoamperometry was used for the incorporation of the Ni nanoparticles on the PANI matrix. The micrographs obtained (Fig. 7a) showed a nanofibrous morphology of PANI. From the Ni-PANI/FTO sample presented in Fig. 7b,
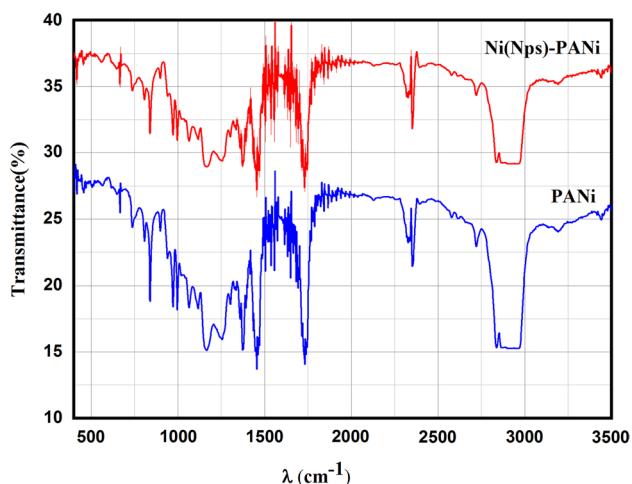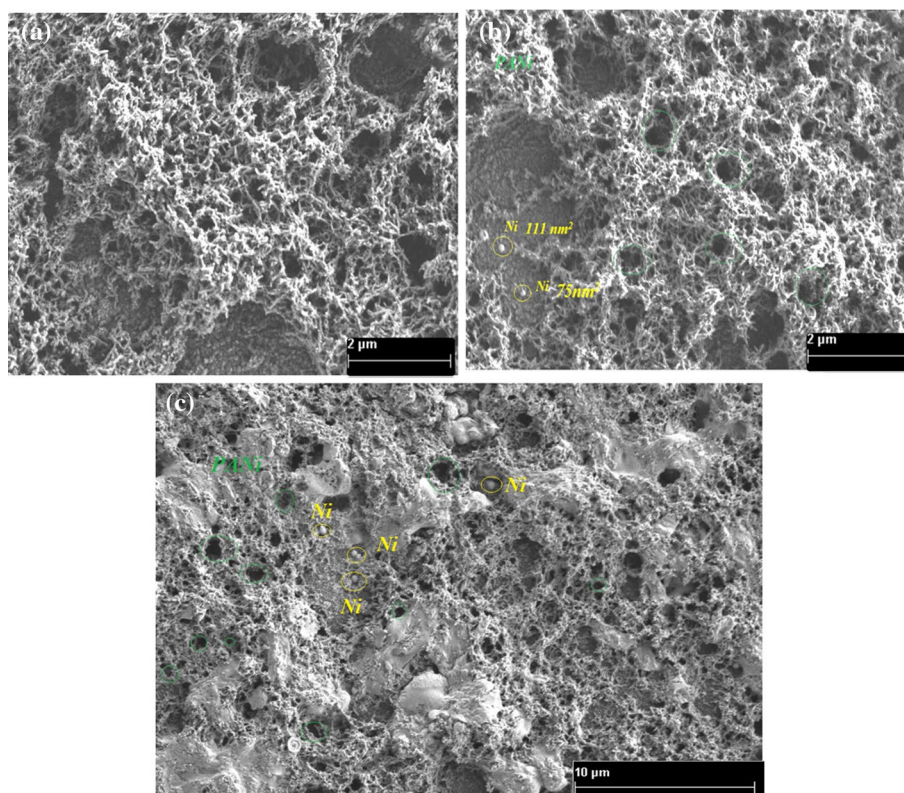

Fig. 6 FTIR spectroscopy analysis of PANI and Ni (NPs)-PANI electrodes.

two nanoparticles of Ni (circled in yellow), with an area of 72 nm^2 and 111 nm^2, are shown deposited on the FTO substrate directly where there is no deposited PANI. Moreover, the porosity of the PANI layer shown in the densely deposited places is determined by the largest pores (examples circled in blue) of a few hundred square-nanometers (μm^2) to the smallest pores of a few square-nanometers (nm^2). This result is in reasonable agreement with other studies.[39] Our results indicate the dispersion of small nanoparticles through the dense PANI layer. The improvement in the sensing parameters could be explained by the dispersion of Ni in the PANI matrix, which provides better surface area and catalytic sites.[40]

The nanocomposite surface was analyzed using the AFM. According to the results illustrated in Fig. 8, it should be noted that the root-mean-square roughness of Ni (NPs) - (63.444 nm) is greater than was observed for the PANI layer (18.038 nm).

Electrochemical Measurements

The Ni (NPs)-PANI electrode was successfully demonstrated. Electrocatalytic performance for glucose detection is also reported.

Figure 9 depicts the CVs of FTO. The solution containing 0.1 M NaOH was used for the measurement of PANI and Ni (NPs)-PANI. Thus, according to the results obtained, no
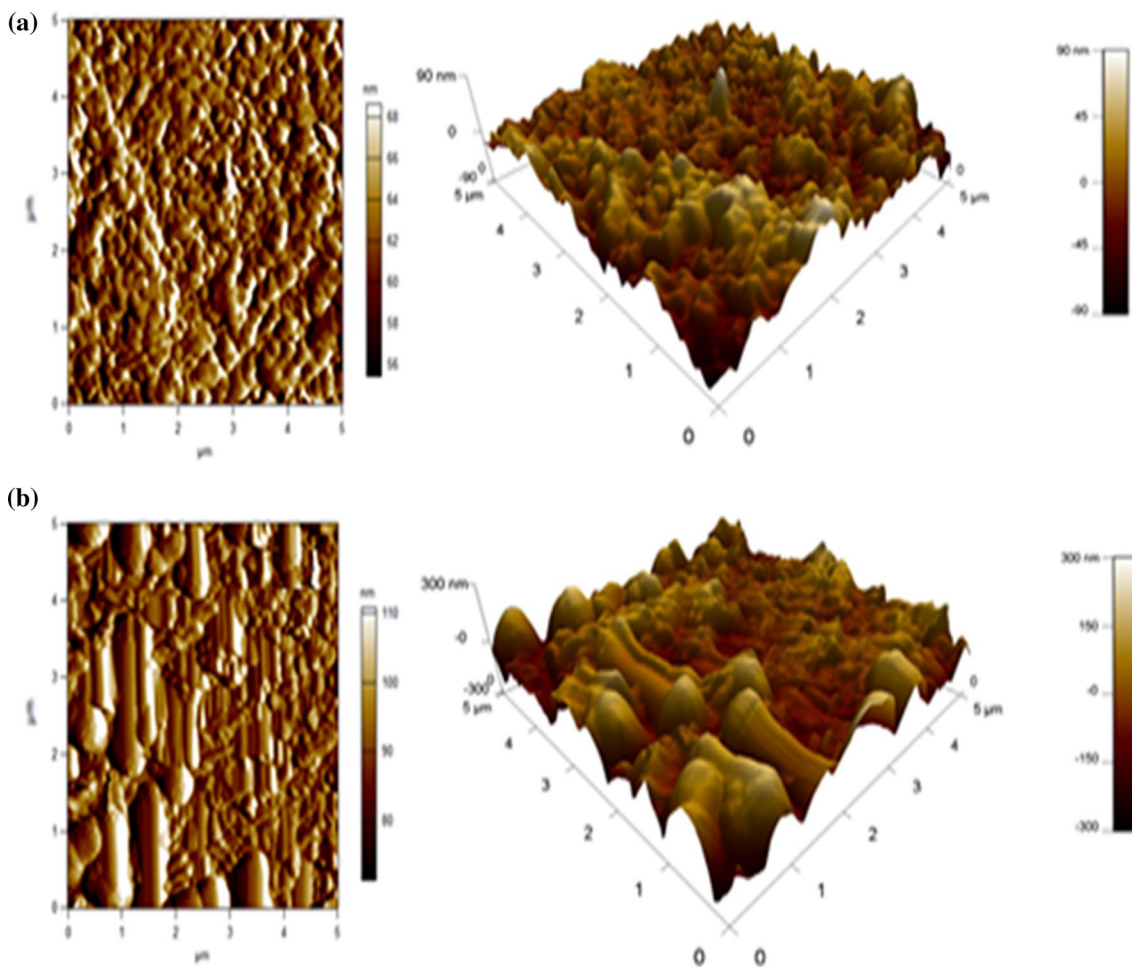
Fig. 7 SEM micrographs of (a) PANI, (b) Ni (NPs)-PANI nanocomposite, (c) at different aggrandizement.

Fig. 8 AFM images (2D, 3D) of the thin layer of (a) PANI and (b) Ni (NPs)-PANI electrodes.

current was observed for FTO and PANI in the potential range of interest. This indicates the absence of the oxidation-reduction process on the surface of the FTO and PANI substrate due to deprotonation of PANI in alkaline solution.[21] Moreover, it should be noted that the electrochemical oxidizing current increases when integrating the Ni, indicating high sensitivity.[41]

Ni (NPs)-PANI as an Electrode for Electrocatalytic Oxidation of Glucose

After depositing the Ni (NPs)-PANI nanocomposite, the electroactivation step was carried out. This step, which consists of subjecting the nanocomposite surface to a succession of oxidation-reduction reactions, promotes an increase in the oxidation state of the metal at the surface. Figure 10a depicts the results of consecutive CVs of the Ni (NPs)-PANI electrode in 0.1 M NaOH solution recorded at 25 mV s^{-1}, 10 cycles. The first positive potential sweep shows similar properties as the pure Ni.[41] As the number of cycles increases,
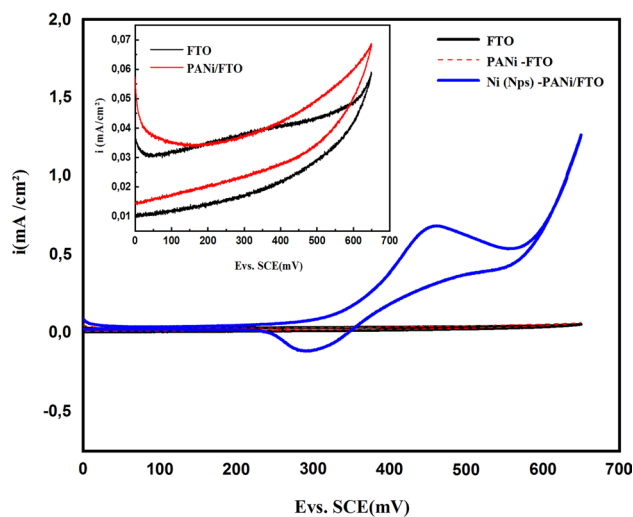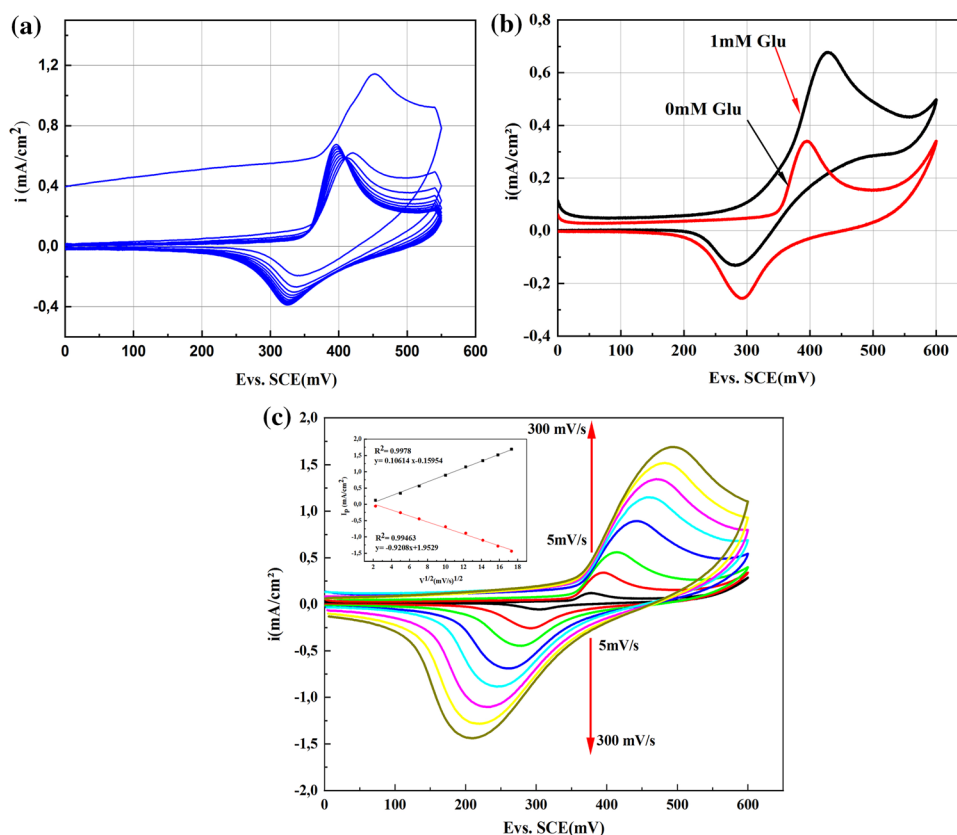

Fig. 9 Cyclic voltammogram (CV) of FTO, PANI and Ni (NPs)-PANI in aqueous solutions containing 0.1 M NaOH + 1 mM glucose at 25 mV s^{-1}. Zoom of the CVs of FTO and PANI values in the inset.

Fig. 10 CV profiles of Ni (NPs)-PANI /FTO electrode observed in 0.1 M NaOH (a) at 25 mV s^{-1}, and 10 cycles (b) without and with glucose and (c) at different scan rates.

the oxidation current peak increases significantly, indicating the formation of the two phases, α-Ni (OH)$_2$ and β-Ni (OH)$_2$, and the increase in inactive sites. Moreover, the electroactivation step will increase the proportion of the Ni in the β-Ni (OH)$_2$ phase (which is most favorable to the detection of glucose), and ensures the formation of the pair Ni(OH)$_2$/ NiOOH.[42]

The electrochemical behavior of Ni (NPs)-PANI nanocomposite in NaOH (0.1 M) with/without glucose is shown in Fig. 10b. In the absence of glucose, a well-defined pair of redox peaks corresponding to the Ni^{3+}/Ni^{2+} couple has appeared. However, in the presence of glucose (1 mM), the peak potential's anodic shift has been observed with enhanced oxidative peak current. Although, the cathodic peak current kept decreasing slightly, indicating irreversible electrochemical oxidation. The electrooxidation of glucose with Ni^{3+} is the reason for the enhanced anodic current.[42]

Mechanism of Oxidation of Glucose by Ni (NPs)-PANI

The Ni^{2+} in Ni (NPs)-PANI nanocomposite will be converted to Ni(OH)$_2$ in 0.1 M NaOH, and then Ni(OH)$_2$ is electrochemically oxidized to NiOOH under alkaline conditions. Glucose is oxidized to gluconolactone by NiOOH, and Ni(OH)$_2$/NiOOH acts as an electron transfer agent during the process of oxidation.[43] The whole process for glucose

oxidation by the redox couple Ni(OH)$_2$/NiOOH is presented in Eqs. 2–4.

$$Ni^{2+} + 2OH^- \rightarrow Ni(OH)_2 \tag{2}$$

$$Ni(OH)_2 + OH^- - e^- \leftrightarrow NiOOH \tag{3}$$

$$NiOOH + glucose \rightarrow Ni(OH)_2 + glucolactone$$

Figure 10c illustrates the mechanism of glucose detection by a surface-controlled process. The obtained results revealed a very high correlation coefficient (0.997 and 0.994) corresponding to the current density of oxidation and reduction peaks at different scan rates, respectively, which indicates a diffusion-controlled redox reaction using the basic electrolyte and the Ni (NPs)-PANI electrode.[38,43]

Figure 11a reveals the CV responses of Ni (NPs)-PANI nanocomposite in 0.1 M aqueous NaOH solution with different glucose concentrations at a 25 mV s^{-1} scan rate. As can be seen, the results indicated a significant increase in the current at different injected concentration of glucose, which facilitates electron transfer and accelerates mass transport.[45]

Therefore, the linear regression of the current versus the glucose concentration is described by the following equation: y = 397.24 + 0.2788*x where y is the current in mA

Fig. 11 (a) Ni (NPs)-PANI electrode evaluation as a function of glucose concentration, (b) the calibration curve shows a linear correlation.
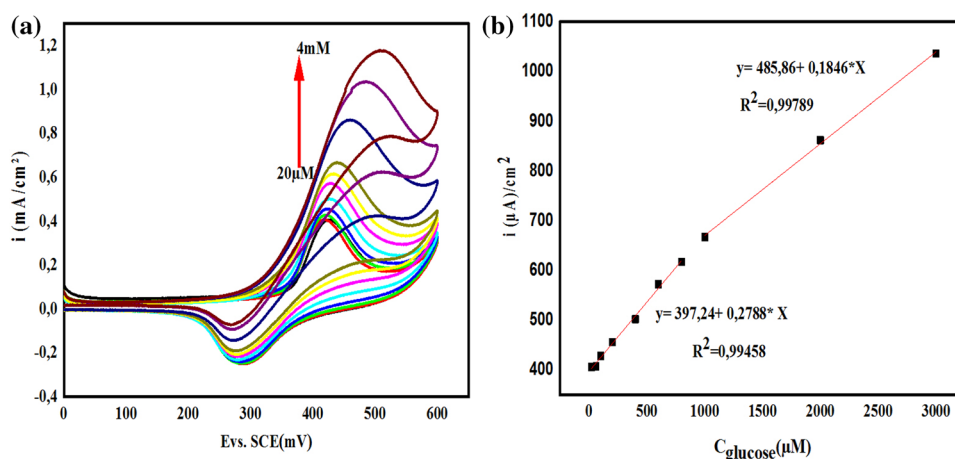

Table I Summary of parameters of Ni (NPs)-PANI electrode.

Materials	Solution (M)	LOD (µM)	Sensitivity (μAmM^{-1}cm^{-2})	Linear range (mM)
Ni (NPs)-PANI	0.1 NaOH	1.0	278.46	0.0–1.0

cm^{-2} and x is the glucose concentration in µM with a corresponding coefficient of determination (R^2 = 0.99458).

The observed sensitivity from Fig. 11b is 278.8-µA cm^{-2} mM^{-1}. According to our experiments, the lowest concentration of glucose was 1.0 µM at a signal-to-noise ratio of 3. The analytical parameters of the Ni (NPs)-PANI electrode is shown in Table I. Also, Table II presents the analytical performance of the electrode. As observed, our results are comparable to those obtained by other previously reported works to determine glucose.

Sensor Selectivity of the Ni (NPs)-PANI Electrode

Anti-interfering ability is one of the most important parameters of an amperometric sensor. It is partially non-selective toward other oxidizable species coexisting with glucose.[46] In the present work, the selectivity of the Ni (NPs)-PANI was measured at an applied potential of +0.5 V, to the sequential addition of 1 mM or 0.5 mM of glucose and 0.01 mM of a few interfering species that coexist with glucose

in human blood, including ascorbic acid (AA), sucrose (Suc), and potassium chloride (KCl). The obtained results are illustrated in Fig. 12. Compared to the drastic increase in responses in the presence of glucose; the addition of the interferant species show no significant effect on the current responses, which could be explained by the high selectivity of the Ni (NPs)-PANI electrode, and thus confirming better selectivity of this electrode at a fast-enough response time of 3 s towards glucose oxidation.

In terms of reproducibility, the implemented sensor was evaluated based on the measurement of glucose oxidation using three Ni (NPs)-PANI electrodes with the same modifications and measurement conditions, and based on the relative standard deviation value of 2.5%, the obtained results revealed acceptable reproducibility.

Conclusions

In this study, a Ni (NPs)-PANI material-based electrochemical glucose sensor has been successfully synthesized by electrodeposition. The PANI was applied as a support to load the Ni nanoparticles, and had an important role in electronic transmission. The Ni (NPs)-PANI electrode displayed high sensitivity (278.46 µAmM^{-1}cm-^{2}), with a wide linear range from 0.02 to 1 mM. The proposed electrode-based sensor demonstrated high selectivity for glucose detection. All results of the present study show that the Ni (NPs)-PANI

Table II A comparison of glucose sensing parameters using non-enzymatic glucose sensors.

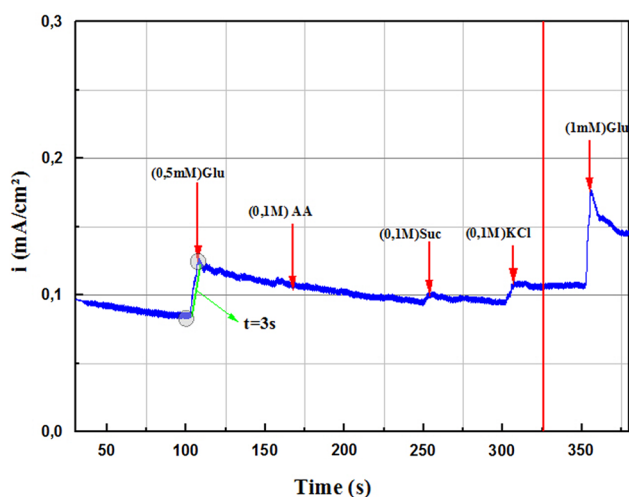| Material	A linear range (mmol/L)	LOD (µmol/L)	Sensitivity (µA/(cm^2 mM))	Ref
AuNPs/PANI/CC	0.01–10.0	3.08	150	42
NiO/6% PANI	0-0.1	0.19	606.13	43
Ni nanowire arrays	0.00005 –7	0.1	1043	44
Ni (NPs) -PANI	0 .02-4	1.0	278.46	This work

Fig. 12 Amperometric response of the Ni (NPs)-PANI to the sequential addition of 0.5mM or 1mM glucose and 0.01 mM of a number of interfering species: AA, Sac, KCl, at 0.50 vs SCE (mV).

electrode is a promising candidate for developing cheap, stable, and sensitive non-enzymatic glucose sensors.

Conflict of interest The authors declare no conflict of interest.

References

1. P. Martinkova and M. Pohanka, *Anal. Lett.* 48, 2509 (2015).
2. N. Ch and R. Paily, *Micromachines* 5, 722 (2014).
3. D. Albanese, A. Sannini, F. Malvano, R. Pilloton and M. Matteo Di, *Food Anal. Methods* 7, 1002 (2013
4. D. Espes, M. Martinell, H. Liljebäck and P.O. Carlsson, *Curr. Diab. Rep.* 15, 12 (2015).
5. E. Nohra, S. Buckman, K. Bochicchio, J. Chamieh, S. Reese, C. Merrill and G.V. Bochicchio, *Contemp. Clin. Trials* 50, 1 (2016).
6. L. Chen, L. Liu, Q. Guo, Z. Wang, G. Liu, S. Chen, and Hou, H. *RSC advances* (2017).
7. T. Sridara, J. Upan, G. Saianand, A. Tuantranont, C. Karuwan and J. Jakmunee, *Sens* 20, 808 (2020).
8. N. Singer, R.G. Pillai, A.I.D. Johnson, K.-D. Harris and A.B. Jemere, *Microchim. Acta* 187, 196 (2020).
9. G. Wang, X. He, L. Wang, A. Gu, Y. Huang, B. Fang and X. Zhang, *Microchim. Acta* 180, 161 (2012).
10. K. Dhar and D.R. Mahapatra, *Microchim. Acta* 185, 1 (17).
11. D.W. Hwang, S. Lee, M. Seo, and T.D. Chung, *Anal Chim. Acta* 1033, 1 (2018).
12. X. Niu, X. Li, J. Pan, Y. He, F. Qiu and Y. Yan, *RSC Adv* 6, 84893 (2016)
13. H. Shu, L. Cao, G. Chang, H. He, Y. Zhang and Y. He, *Electrochim. Acta* 132, 524 (2014).
14. T. Unmussig, A. Weltin, S. Urban, P. Daubinger, G.A. Urban and J. Kieninger, *J. Electroanal. Chem.* 816, 215 (2018).
15. C.H. Wang, S.W. Lee, C.J. Tseng, J.W. Wu, I.M. Hung, C.M. Tseng and J.K. Chang, *J. Alloy Compd* 615, S496 (2014).
16. H. Yang, Z. Wang, Q. Zhou and C. Xu, *J. Hou Microchim. Acta* 186, 631 (2019).
17. D. Lakhdari, A. Guittoum, N. Benbrahim, O. Belgherbi, M. Berkani, Y. Vasseghian and N. Lakhdari, *Food Chem. Toxicol.* 151, 112099 (2021).
18. R. Wang, X. Liang, H. Liu, L. Cui, X. Zhang and C. Liu, *Microchim Acta.* 185, 331 (2018).
19. J.H. Kim, J.H. Cho, G.S. Cha, C.W. Lee, H.B. Kim and S.H. Paek, *Biosens. Bioelectron.* 14, 907 (2000).
20. A.G. MacDiarmid and A.J. Epstein, *Synth Met* 69, 85 (1995).
21. B. Malhotra, C. Dhand, N. Dwivedi, S. Mishra, P. Solanki, V. Mayandi, R.W. Beuerman, S. Ramakrishna and R. Lakshminarayanan, *Nanobiosens. Dis. Diagn.* 4, 25 (2015).
22. X. Gao, X. Du, D. Liu, H. Gao, P. Wang and J. Yang, *Sci. Rep.* 10, 1365 (2020).
23. G. Wu, X. Song, Y.F. Wu, X. Chen, F. Luoa and X. Chen, *Talanta* 105, 379 (2013).
24. X. Niu, M. Lan, H. Zhao and C. Chen, *Anal. Chem.* 85, 3561 (2013)
25. S. Ci, T. Huang, Z. Wen, S. Cui, S. Mao, D.A. Steeber and J. Chen, *Biosens. Bioelectron.* 54, 251 (2014).
26. F.J. Garcia-Garcia, P. Salazar, F. Yubero, A.R. Gonzalez-Elipe, *Electrochim. Acta* 201, 38 (2016).
27. Y. Miao, L. Ouyang, S. Zhou, L. Xu, Z. Yang, M. Xiao and R. Ouyang, *Biosens. Bioelectron.* 53, 428 (2014).
28. K. Dhara and D.R. Mahapatra, *Microchim. Acta* 185, 41 (2017).
29. H. Liu, X. Wu, B. Yang, Z.H. Li, L. Lei and X. Zhang, *Electrochim. Acta* 174, 745 (2015).
30. Z. Cui, H. Yin, Q. Nie, D. Qin, W. Wu and X. He, *J. Electroanal. Chem.* 757, 51 (2015).
31. H. Tian, M. Jia, M. Zhang, J. Hi, *Electrochim. Acta.* 96, 285 (2013).
32. A.A. Ensafi, N. Ahmadi and B. Rezaei, *Sens. Actuators. B Chem* 239, 807 (2017).
33. D. Roy, A.K. Das, R. Saini, P.K. Singh, P. Kumar, M. Hussain, A. Mandal and A.R. Dixit, *Mat. Manuf. Process.* 32, 365 (2017).
34. D.H. Ninh, T.T. Thao, P.D. Long and N.N. Dinh, *Open J. Org. Polym. Mat.* 6, 30 (2016).
35. A.A. Hermas and M.A.Salam, *Prog. Org. Coat.* 77, 403 (2014).
36. J. Wang, Y.G. Ning, Y.F. Wen, Y. Wen, T. Dong, D.M. Wang, J.M. Chen and L.J. Zhang, *Z. Phys. Chem.* 227, 89 (2013).
37. L. Jia, X. Wei, L. Lv, X. Zhang, X. Duan, Y. Xu and J. Wang, *Electrochim. Acta* 280, 315 (2018).
38. U. Sarac, M. Kaya and M. Celalettin Baykul, *Turk. J. Phys.* 41, 536 (2017).
39. J. Laska and J. Widlarz, *Polym* 46, 1485 (2005).
40. S.H. Kazemi, M.A. Kiani, R. Mohamadi and L. Eskandarian, *Bull. Mat. Sci.* 375, 1001 (2014)
41. C.O. Baker, X. Huang, W. Nelson and R.B. Kaner, *Chem. Soc. Rev.* 46, 1510 (2017)
42. K.J. Babu, T. Rajkumar, D.J. Yoo, P. Siew-Moi and G. Gnana Kumar, *ACS Sustain. Chem. Eng.* 6, 16982 (2018)
43. A.M. Ahmed, S.Y. Sayed, G.A. El-Nagar, W.M. Morsi, M.S. El-Deab and El-B.E. Anadouli, *J. Electroanal. Chem.* 835, 313 (2019).
44. L. Qin, L. He, J. Zhao, B. Zhao, Y. Yin and Y. Yang, *Sens. Actuators B* 240, 779 (2017).
45. Xu. Mengli, S. Yonghai, Y. Yihan, G. Coucong, S. Yuan, W. Linyu and W. Li, *Sens. Actuators B* 252, 1187 (2017).
46. A. Mohamed Azharudeen, R. Karthiga, M. Rajarajan and A. Suganthi. *Arabian J. Chem.* 13, 4053 (2020).